



THE UNIVERSITY *of* EDINBURGH

Edinburgh Research Explorer

A competing risks model explains hierarchical spatial coupling of measles epidemics en-route to national elimination

Citation for published version:

Lau, M, Alexander, B, Hannah, K, Caudron, Q, Shaw, D, Metcalf, J, Bjørnstad, O & Grenfell, B 2020, 'A competing risks model explains hierarchical spatial coupling of measles epidemics en-route to national elimination', *Nature Ecology & Evolution*. <https://doi.org/10.1038/s41559-020-1186-6>

Digital Object Identifier (DOI):

[10.1038/s41559-020-1186-6](https://doi.org/10.1038/s41559-020-1186-6)

Link:

[Link to publication record in Edinburgh Research Explorer](#)

Document Version:

Peer reviewed version

Published In:

Nature Ecology & Evolution

General rights

Copyright for the publications made accessible via the Edinburgh Research Explorer is retained by the author(s) and / or other copyright owners and it is a condition of accessing these publications that users recognise and abide by the legal requirements associated with these rights.

Take down policy

The University of Edinburgh has made every reasonable effort to ensure that Edinburgh Research Explorer content complies with UK legislation. If you believe that the public display of this file breaches copyright please contact openaccess@ed.ac.uk providing details, and we will remove access to the work immediately and investigate your claim.



A competing risks model explains hierarchical spatial coupling of measles epidemics *en-route* to national elimination

Max SY Lau^{1,*,}, Alexander D Becker^{2,*}, Hannah M Korevaar², Quentin Caudron², Darren J Shaw⁴, C. Jessica E. Metcalf², Ottar N Bjørnstad³, Bryan T Grenfell^{2,5}

1. Department of Biostatistics and Bioinformatics, Rollins School of Public Health, Emory University, Atlanta, Georgia, 30322, USA

2. Department of Ecology and Evolutionary Biology, Princeton University, New Jersey, 08544, USA.

3. Center for Infectious Disease Dynamics, Department of Biology, Pennsylvania State University, University Park, Pennsylvania, 16802, USA.

4. Royal (Dick) School of Veterinary Studies & The Roslin Institute, University of Edinburgh, Easter Bush Campus, Roslin, Midlothian, EH25 9RG.

5. Fogarty International Center, National Institutes of Health, Bethesda, MD 20892, USA

Corresponding author

*Equal contribution

Abstract

Apart from its global health importance, measles is a paradigm for low-dimensional mechanistic understanding of local nonlinear population interactions. A central question for spatio-temporal dynamics is the relative role of hierarchical spread from large cities to small towns and ‘metapopulation’ transmission among local small population clusters in measles persistence. Quantifying this balance is critical to planning regional elimination and global eradication of measles. Yet, current gravity models do not allow a formal comparison of hierarchical *versus* metapopulation spread. We address this gap with a competing-risks framework, capturing the relative importance of competing sources of reintroductions of infection. We apply the method to the uniquely spatio-temporally detailed urban incidence data set for measles in England and Wales (available in the *Supporting Materials*), from 1944 to the infection’s vaccine-induced nadir in the 1990s. We find that despite the regional influence of a few large cities (e.g. London and Liverpool) metapopulation aggregation in neighboring towns and cities plays an important role in driving national dynamics in the prevaccination era. As vaccination levels increased in the 1970s and 80s, the signature of spatially predictable spread diminished: increasingly, infection was introduced from unidentifiable random sources possibly outside regional metapopulations. The resulting erratic dynamics highlight the challenges of identifying shifting sources of infection and characterizing patterns of incidence in times of high vaccination coverage. More broadly, the underlying incidence and demographic data, accompanying this paper, will also provide a significant resource for exploring nonlinear spatiotemporal population dynamics.

Introduction

The widespread use of an effective vaccine since the mid 1960s has greatly reduced the global circulation of measles. However, the virus continues to be a major cause of death among young children in sub Saharan Africa^{1,21}. Even in many countries with previously effective control, the recent re-emergence of measles, often fueled by vaccine hesitancy, further confirms measles as a significant public health problem globally^{2,3}. A simple natural history of infection, and reliable and detailed case notification across an array of settings^{4,5}, also makes measles one of the best-documented spatiotemporal disease systems, in particular, and ecological consumer-resource model system more

generally^{6,7}. However, significant gaps still exist in our understanding of measles spread; we address these lacunae here.

Measles dynamics before and since the introduction of mass-vaccination are particularly richly documented by historical notifications in England and Wales (E&W; Figure S1 and data in *Supporting Materials A and E*). Before widespread vaccination, measles epidemics in E&W (and many developed countries) were characterized by highly seasonal periodic (often biennial) cycles in large cities and erratic outbreaks driven by extinction-recolonization processes in smaller places (Figure S1a)^{4,8}. The *Critical Community Size* (CCS) of about 300,000 people for measles in pre-vaccination E&W is the empirically identified threshold required for sustained local chains of infection⁹. In 1960, roughly 16% of the population of England and Wales inhabited 10 big cities above the CCS. Previous studies have identified these as the pacemakers for regional dynamics^{4,8}. The remaining 84% of the population were subdivided among more than 1,000 smaller conurbations and rural areas, with more irregular dynamics. Since its introduction in 1968, vaccination has significantly reduced the magnitude and regularity of epidemics throughout the regional hierarchy¹⁰ (Figure S1a). This trend is accompanied by a decline in local persistence (Figure S1(b)), which was especially marked as vaccination rates increased in the 1980s and regional dynamics became increasingly decorrelated^{4,10}.

At the scale of the metapopulation (here, defined by cities and towns), measles persistence depends on reintroduction of infection following extinction in local small communities. Previous work has stressed the role of hierarchical ‘core-satellite’ spread from large to small conurbations in the pre-vaccination era (Figure 1a), as a particularly clear exemplar of forest-fire-like extinction-recolonization dynamics^{11,12}. This hypothesis is supported by a wavelet phase analysis which reveals spatial waves travelling from core cities (in particular, London and the industrial north-west) to smaller, more peripheral satellite towns and villages (4). However, a deeper understanding of how and to what extent these large cities and other ‘competitor’ infective sources drive the overall disease dynamics is still lacking, particularly as regards the role of local aggregation of communities below the CCS in regional metapopulations, a mechanism hereafter referred to as *local metapopulation persistence* (LMP) (Figure 1b).

The central challenge is to model spatial coupling in a more general sense, to quantify metapopulation synchrony across variable vaccination rates. Inspired by transportation theory¹³, Murray and Cliff¹⁴ first proposed that such interactions may be captured by gravity models. This formulation assumes that movement among locales decays with distance but increases in a generalized, bilinear fashion with ‘donor’ and ‘recipient’ population sizes. Gravity models and their extensions have provided useful insights into the spatial interactions of many human and non-human disease systems and facilitated disease predictions and explorations of control^{8,15,16}. However, in the absence of independent covariates describing human movement (a particularly thorny issue for childhood infections like measles, as historical movement data on children are sparse), model inference - in particular, simultaneous inference of epidemic trajectories and spatial coupling- is notoriously difficult; researchers have thus resorted to less interpretable non-mechanistic approaches (e.g., performing approximation using Gaussian processes)^{8,17,18}. While they capture a partial picture of measles dynamics, these methods notably do not allow for a direct quantification of spatial coupling and systematic titration of the relative importance of different sources of reintroduction of infection. We address this gap by formulating a semi-mechanistic Absence-Presence-Absence model in a competing-risks framework which focuses explicitly on modelling the *reintroduction* of infections that are

characteristic of small populations (see Methods and Figure 1c). Our approach enables a direct quantification of spatial coupling and allows us to further titrate the relative importance of different sources (e.g. LMP versus core-satellite) of reintroduction (i.e., a *competing-risks framework*¹⁹).

We use this model in tandem with the exhaustive data set of measles incidence across E&W to dissect and quantify the importance of competing sources of reintroductions of infection in pre-vaccination era. We further identify the changing roles of regional gravity coupling and geographically erratic dynamics in seeding epidemics as mass vaccination was rolled out from the late 1960s onwards.

Results

Regional dynamics pre-vaccination

Pre-vaccination epidemics in cities above the CCS were largely self-sustaining and insensitive to transient imported infections due to spatial coupling^{8,20}; also, extinctions and reintroductions in these larger populations are by definition uncommon. To quantify spatial coupling, we therefore focus our analysis on the timings of epidemics in all populations well below the CCS (872 places; N<100,000), whose dynamics should carry a robust signal of coupling.

We fit the semi-mechanistic Absence-Presence-Absence model (see *Methods*) to biweekly incidence data during the pre-vaccination era (1944-1964) in England and Wales (E&W), from the 872 smallest towns and cities (comprising 93% of all locations). The other 82 cities (N>100,000) inform the analysis as additional donors of infection. Using the estimated model, we forward simulate the timings of reintroductions and extinctions of each of the places. We compare observed and simulated data, based on six key aspects of measles dynamics. Figure 2 shows that our estimated model accurately captures all these key aspects of dynamics. We tested the overall inferential framework by assessing performance on simulated data from a detailed metapopulation gravity model⁸ (see *Supporting Materials C*).

Importance of Core-satellite, LMP and Random Seeding

We calculate the relative risk of reintroduction between aggregate ('predictable') inter-population *gravity-driven coupling* (i.e. core-satellite plus LMP) versus *unidentifiable random seeding* (i.e. any sources of reintroductions that are not captured explicitly by the gravitational components of our model structure) for each location (see Figure 1a-b). Note that, since reintroductions are defined to only occur during local extinctions (Figure 1c), local dynamics may contribute insignificantly to any unidentifiable seeding in our context. Figure 3a shows the aggregate distribution across E&W for the entire pre-vaccination time-series, suggesting that about 90% of the introductions can be accounted for by gravity coupling in this era. To get a more spatially-resolved picture we use *local indicators of spatial association* (LISA²¹), capturing the *relative* importance of 'predictable' versus random spread. The LISA analysis shows that random spread is significantly more important in 'peripheral' areas (Cornwall, mid- and North Wales and East Anglia) compared to the rest of E&W (Figure 3b); isolated coastal areas feature especially in this group²². Despite the relative importance of erratic dynamics in

the periphery compared to the rest of E&W, gravity-driven dynamics, absolutely speaking, remain dominant in these regions in the pre-vaccination era. Norwich and its environs, which became out of phase with the overall national trend during the 1950s, exhibiting even-year major epidemics, also appear as an outlier in terms of inferred metapopulation coupling.

The estimated model allows sampling of the source of infection for each reintroduction (see *Methods* and *Supporting Materials BII*). We can therefore quantify the relative importance for each recipient community of each of the core cities, conditional on the sampled reintroductions of infections at each recipient community due to gravity coupling. Figure 3c shows the most influential donor city (among major core cities and other places) for each location (i.e. the donor city that is responsible for the largest proportion of reintroductions). The prominent influence of London on smaller towns around its periphery is broadly consistent with the hierarchical waves discussed in ⁴. Furthermore, Figure 3c-d show that, apart from the impact of a few core cities, LMP is an important driver in triggering reintroduction with a median distance of transmission of 10.3 kilometers. The average distance to the nearest neighboring community in the data is 7.0 km (median: 5.3km, IQR: 3.1km, 9.6km). LMP thus roughly-speaking extends out to 2nd nearest neighbors in E&W's spatial network.

Gravity-driven versus Geographically Erratic Spread over the history of vaccination

To investigate the changing roles of predictable gravity coupling (i.e. core-satellite plus LMP) and unidentifiable seeding following introduction of vaccination (Figure S1 and 1), we fit our model to 5-year periods spanning the pre-vaccination era and the gradual increase in vaccination coverage during the 1970s and 80s. For consistent spatial comparison through time, we use the post-1974 data aggregation (354 locations) to correct for changes in boundaries between the 1940s and 1990s (see *Supporting Materials A* for our method of aggregating pre-vaccination data). To more explicitly measure the effect of unidentifiable sources relative to spatially predictable spread, we allow for different unidentifiable seeding parameters during different periods (see *Methods* and *Supporting Materials B*). Figure 4a depicts the location-wise distribution of risk due to spatially predictable and unidentifiable random seeding. It shows that the strength of gravity coupling diminished gradually with increasing vaccine coverage, while unidentifiable random seeding played an increasingly and progressively dominant role. Increased vaccination drove an increase in the CCS (Figure S1) and an overall decline in gravity-driven spread (Figure 4b).

The increase in spatially erratic spread is also associated with a decay in both local and regional spatial synchrony in the vaccine era ⁴ (Figure 4c). Prior to vaccination the regional synchrony, measured by a non-parametric spatial correlation function (ranges between 0 and 1, with 1 representing complete spatial synchrony) ²⁴, across E&W was 0.35, with a local above-average correlation of 0.65 that extended to a distance of 125km. This collapsed to region-wide synchrony of 0.03 in the 90's with an above-average local synchrony of 0.06 (Figure 4c). Importantly, the effective breakdown of the consumer-resource metapopulation could reinforce regional persistence through spatial transmission among asynchronous local epidemics; this could significantly hamper the likelihood of elimination, even at high vaccine uptake levels ²⁵.

Discussion

Characterizing drivers of measles outbreaks has important public health implications, in terms of optimizing vaccine deployment to achieve regional, then global elimination of infection. Recurrent

measles outbreaks also illuminate fundamental questions regarding nonlinear population dynamics. Our analysis of the full urban hierarchy of measles outbreaks over 50 years in E&W sheds new light on regional dynamics and the impact of vaccination on them.

Inferring epidemiologically-relevant local and regional movement (mainly of children for pre-vaccination measles), is a classic challenge in epidemiology. Here we extend the existing rich body of work by developing a metapopulation framework that allows us to titrate the relative importance of different sources of reintroduction of infection, in the absence of explicit movement data. Rooted in transportation theory¹³, the gravity model has been modified and widely applied in epidemiological and ecological studies for understanding the spatial dynamics of populations. The gravity framework for measles developed by Xia *et al.*⁸ provided important insights, leveraged in subsequent gravity-themed models for measles¹⁷ and other infections^{14–16,18}. However, due to its over-parameterized formulation¹⁷ (especially given the absence of explicit information on movement drivers; see *Supporting Materials B*), direct and accurate quantification of spatial coupling and titration of the importance of different sources of reintroduction are difficult¹⁷. Building on previous work, we adapted the general concept of competing-risk frameworks¹⁹ and derived a patch-level Absence-Presence-Absence model, which allows us to accurately capture the signal of spatial coupling and explicitly quantify the importance of different sources for reintroductions across multiple eras of transmission.

Infective sparks of measles are conventionally assumed to spread from big cities like London to their nearby smaller conurbations, consistent with core-satellite dynamics. Our results give the most detailed quantification to date that local metapopulation persistence (LMP) is also important in the spatial dissemination and regional persistence of infection²⁶. LMP will be a critical challenge to tackle in designing control strategies for elimination. Our analysis also highlights that the vaccine-driven decorrelation of local epidemics is associated with a weakening of predictable gravity-driven spread and an increase in dominance of erratic reintroductions from unidentifiable origins (consistent with genetic evidence that international importations of infection has become more influential in the vaccination era^{27,28}). The transitions in spatial dynamics revealed in the unique E&W measles dataset illuminate how regional and global elimination of infection is critically influenced by the interaction between changing local nonlinear clockworks, aggregate spatial transmission rates and the resulting emergent spatiotemporal dynamics. Understanding these interactions is increasingly urgent in the face of secular declines in vaccination and re-establishment of measles endemism (seen post-1994 in the E&W²⁹).

As with any surveillance stream, our data set is subject to a number of approximations (see *Supporting Materials A*); however, we believe that our overall results are robust to these (see *Supporting Materials A, B*). A generic problem for projecting historical dynamics to the future are secular changes in system parameters. For measles, a particularly knotty example is behavior change: the large pre-vaccination era epidemics analyzed here did not drive any major change in behavior for disease-avoidance; in the present era, behavior change during epidemics (and hence modulation of transmission) is more likely³⁰. A powerful extension of historical analyses to allow for social and demographic variation in transmission would be the integration of epidemiological models with estimates of population susceptibility from periodic age-serological surveys³¹.

Notwithstanding these complexities, there is considerable further scope to leverage historical data sets, such as presented here, to illuminate a range of both specific public health and general nonlinear population dynamic questions³². For example, digitization of the full E&W Registrar General and OPCS Weekly Reports back to 1855, of which the measles data presented here are a small part, would generate rich dynamical dividends on multiple important infections and questions.

Methods

Descriptive statistical methods. Standard methods (wavelets⁴, non-parametric spatial correlation²⁴, LISA²¹) are referenced in the text. All analyses were performed in R version 3.5.1.

Competing risks framework with an Absence-Presence-Absence model. The competing risks framework aims to quantify spatial coupling processes beyond existing methods^{8,17,20}. We do not model the local epidemic trajectories as considered in Xia *et al.*⁸ (see *Supporting Materials C* for a simulation study with our framework). Our approach instead focuses on the local absence-presence-absence (A-P-A) of infection via a Susceptible-Infected-Susceptible (SIS)-like patch-level model^{33,34} where a spatial infection event (i.e., transition from Absence (A) to Presence (P)) corresponds to a *reintroduction* and the transition from P to A corresponds to a local *extinction* event (Figure 1c). As reintroductions, defined to occur during local extinctions (Figure 1c), are mostly due to the effect of (external) spatial coupling instead of (internal) seedings of local dynamics, our approach enables a direct quantification of spatial coupling. The transition from P to A is governed by a waiting time distribution that depends on introduction and susceptible recruitment rates¹⁸. Each location is classified as ‘Absent’ (and susceptible to reintroduction) in any given biweek if there were no cases of measles at the time or ‘Present’ if measles was reported (see *Supporting Materials B*). We embed our model within an explicit gravity network among all cities/towns. In particular, the force of reintroduction of infection exerted on a particular town/city j by a city/town k at time t is

$$p(j, k, t) = \beta \times I_{k,t}^{\alpha_1} \times N_{j,t}^{\alpha_2} \times \frac{1}{d_{k,j}^{\rho}},$$

where $d_{k,j}$, $I_{k,t}$ and $N_{j,t}$ are the distance between k and j , the number of measles cases in k and the population in j at time t respectively. We also consider unidentifiable background (‘random’) sources of reintroduction of infection with rate τ , capturing any sources of reintroductions that are not captured explicitly by the gravitational components of our model structure. We also formally capture the effect of local susceptibility by a parameter η (see *Supporting Materials B* for details). Model parameters are inferred using Bayesian inference using either noninformative or informative priors depending on data resolutions (*Supporting Material B*). Note that since reintroductions are defined to only occur during local extinctions (Figure 1c), local dynamics may only contribute insignificantly to any unidentifiable seeding in our context. A link to major code is included in the *Supporting Material*.

Author Contribution

M.S.Y.L. designed research; M.S.Y.L., A.D.B., and B.T.G. performed research; M.S.Y.L. analyzed data; and M.S.Y.L., A.D.B., H.M.K., Q.C., D.J.S., C.J.E.M., O.N.B. and B.T.G. wrote the paper.

Data Availability

Code and measles data are available at https://github.com/msylau/measles_competing_risks.

274
275
276
277
278
279
280

281
282
283
284
285
286
287
288
289

290

291
292

293
294

295
296

297
298

299
300

301
302

Competing interests

None.

Acknowledgments

We thank the RAPIDD Program of the US Department of Homeland Security and the Fogarty International Centre, National Institutes of Health (NIH). H.M.K was also supported by The Eunice Kennedy Shriver National Institute of Child Health & Human Development of the National Institutes of Health under Award Number P2CHD047879. A.D.B. was supported by a National Science Foundation Graduate Research Fellowship.

References and Notes

1. Verguet, S. *et al.* Measles control in Sub-Saharan Africa: South Africa as a case study. *Vaccine* **30**, 1594–1600 (2012).
2. Sabbe, M. Measles resurgence in Belgium from January to mid-April 2011 : a preliminary report. *EuroSurveillance* **16**, 19848 (Avril 2011) (2011).
3. Châtelet, I. P. du, Floret, D., Antona, D. & Lévy-Bruhl, D. Measles resurgence in France in 2008, a preliminary report. *Eurosurveillance* **14**, 19118 (2009).
4. Grenfell, B. T., Bjørnstad, O. N. & Kappey, J. Travelling waves and spatial hierarchies in measles epidemics. *Nature* **414**, 716–723 (2001).
5. Finkenstädt, B. F. & Grenfell, B. T. Time series modelling of childhood diseases: a dynamical systems approach. *J. R. Stat. Soc. Ser. C Appl. Stat.* **49**, 187–205 (2000).
6. King, A. A. & Schaffer, W. M. The Geometry of a Population Cycle: A Mechanistic Model of Snowshoe Hare Demography. *Ecology* **82**, 814–830 (2001).
7. Wilson, H. B. & Hassell, M. P. Host–parasitoid spatial models: the interplay of demographic stochasticity and dynamics. *Proc. R. Soc. Lond. B Biol. Sci.* **264**, 1189–1195 (1997).

- 303 8. Xia, Y. Measles metapopulation dynamics: a gravity model for epidemiological coupling and
304 dynamics. *Am. Nat.* **164**, 267–281 (2004).
- 305 9. Keeling, M. J. & Grenfell, B. T. Disease Extinction and Community Size: Modeling the
306 Persistence of Measles. *Science* **275**, 65–67 (1997).
- 307 10. Bolker, B. M. & Grenfell, B. T. Impact of vaccination on the spatial correlation and persistence
308 of measles dynamics. *Proc. Natl. Acad. Sci.* **93**, 12648–12653 (1996).
- 309 11. Bak, P. *How Nature Works: the science of self-organized criticality*. (Springer Science &
310 Business Media, 2013).
- 311 12. Grenfell, B. & Harwood, J. (Meta)population dynamics of infectious diseases. *Trends Ecol.*
312 *Evol.* **12**, 395–399 (1997).
- 313 13. Erlander, S. & Stewart, N. F. *The Gravity Model in Transportation Analysis: Theory and*
314 *Extensions*. (VSP, 1990).
- 315 14. Murray, G. D. & Cliff, A. D. A Stochastic Model for Measles Epidemics in a Multi-Region Setting.
316 *Trans. Inst. Br. Geogr.* **2**, 158–174 (1977).
- 317 15. Ferrari, M. J. *et al.* A Gravity Model for the Spread of a Pollinator-Borne Plant Pathogen. *Am.*
318 *Nat.* **168**, 294–303 (2006).
- 319 16. Viboud, C. *et al.* Synchrony, Waves, and Spatial Hierarchies in the Spread of Influenza. *Science*
320 **312**, 447–451 (2006).
- 321 17. Jandarov, R., Haran, M., Bjørnstad, O. & Grenfell, B. Emulating a gravity model to infer the
322 spatiotemporal dynamics of an infectious disease. *J. R. Stat. Soc. Ser. C Appl. Stat.* **63**, 423–444
323 (2014).
- 324 18. Bjørnstad, O. N. & Grenfell, B. T. Hazards, spatial transmission and timing of outbreaks in
325 epidemic metapopulations. *Environ. Ecol. Stat.* **15**, 265–277 (2007).

- 326 19. Birnbaum, Z. W. *On the mathematics of competing risks*. (U.S. Dept. of Health, Education, and
327 Welfare, Public Health Service, Office of the Assistant Secretary for Health, National Center
328 for Health Statistics ; for sale by the Supt. of Docs., U.S. Govt. Print. Off, 1979).
- 329 20. Bjørnstad, O. N., Finkenstädt, B. F. & Grenfell, B. T. Dynamics of Measles Epidemics:
330 Estimating Scaling of Transmission Rates Using a Time Series Sir Model. *Ecol. Monogr.* **72**,
331 169–184 (2002).
- 332 21. Anselin, L. Local Indicators of Spatial Association—LISA. *Geogr. Anal.* **27**, 93–115 (1995).
- 333 22. Measles on the Edge: Coastal Heterogeneities and Infection Dynamics.
334 <https://journals.plos.org/plosone/article?id=10.1371/journal.pone.0001941>.
- 335 23. Bjornstad, O. N. *ncf: Spatial Nonparametric Covariance Functions*. (2016).
- 336 24. Bjørnstad, O. N. & Falck, W. Nonparametric spatial covariance functions: Estimation and
337 testing. *Environ. Ecol. Stat.* **8**, 53–70 (2001).
- 338 25. Graham, M. *et al.* Measles and the canonical path to elimination. *Science* **364**, 584–587
339 (2019).
- 340 26. Lloyd, A. L. & May, R. M. Spatial Heterogeneity in Epidemic Models. *J. Theor. Biol.* **179**, 1–11
341 (1996).
- 342 27. Ramsay, M. E. *et al.* The Elimination of Indigenous Measles Transmission in England and
343 Wales. *J. Infect. Dis.* **187**, S198–S207 (2003).
- 344 28. Jin, L., Brown, D. W., Ramsay, M. E., Rota, P. A. & Bellini, W. J. The diversity of measles virus in
345 the United Kingdom, 1992–1995. *J. Gen. Virol.* **78**, 1287–1294 (1997).
- 346 29. Jansen, V. a. A. *et al.* Measles Outbreaks in a Population with Declining Vaccine Uptake.
347 *Science* **301**, 804–804 (2003).

- 348 30. Gastañaduy, P. A. *et al.* Impact of Public Health Responses During a Measles Outbreak in an
349 Amish Community in Ohio: Modeling the Dynamics of Transmission. *Am. J. Epidemiol.* **187**,
350 2002–2010 (2018).
- 351 31. Metcalf, C. J. E. *et al.* Use of serological surveys to generate key insights into the changing
352 global landscape of infectious disease. *Lancet Lond. Engl.* **388**, 728–730 (2016).
- 353 32. van Panhuis, W. G. *et al.* Contagious Diseases in the United States from 1888 to the Present. *N.*
354 *Engl. J. Med.* **369**, 2152–2158 (2013).
- 355 33. Kermack, W. O. & McKendrick, A. G. A Contribution to the Mathematical Theory of Epidemics.
356 *Proc. R. Soc. Lond. Math. Phys. Eng. Sci.* **115**, 700–721 (1927).
- 357 34. Keeling, M. J. & Rohani, P. *Modeling Infectious Diseases in Humans and Animals*. (Princeton
358 University Press, 2008).

359

360

361

362

363 **Figure 1: A schematic illustration of spatial dynamics and persistence of measles a) Core-satellite**
364 **spread of measles. This represents a hierarchical spread of infection from a core city above the**
365 **CCS to its nearby smaller towns/villages. b) Persistence of measles due to local aggregation of**
366 **communities below the CCS in regional metapopulations (hereafter referred to as *local***
367 ***metapopulation persistence, LMP*). Core-satellite spread is effectively directional because back-**
368 **spill does not affect core dynamics while metapopulation spread is potentially bi-directional. c)**
369 **Schematic illustration of the extinction-recurrent epidemic pattern typically observed in a small**
370 **town/city. A *reintroduction/recolonization* time is the time a local epidemic is initiated and**
371 ***extinction* time is when an epidemic ends in a local fade-out.**

372

373 **Figure 2: Fit of the Absence-Presence-Absence model in the competing-risks framework from**
374 **1944-1964. Predictive distributions of key aspects of measles dynamics: 1) the number of**
375 **reintroductions, 2-3) the mean and the standard deviation of epidemic cycles (i.e. times, in the**
376 **unit of biweek, between consecutive reintroductions) , 4) the number of biweeks with zero case**
377 **reports, and 5-6) the mean and the standard deviation of epidemic durations (i.e. times between**
378 **reintroduction and extinction, see also Figure 1c). Grey bands represent 95% credible intervals**
379 **and black dots correspond to the observed data. Locations (cities or towns) are binned equally**
380 **into 40 levels according to their average population size (x-axis shows the upper limit of each**
381 **interval).**

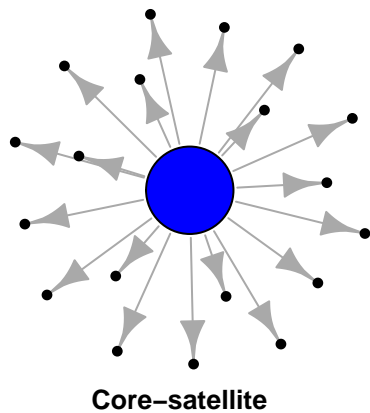
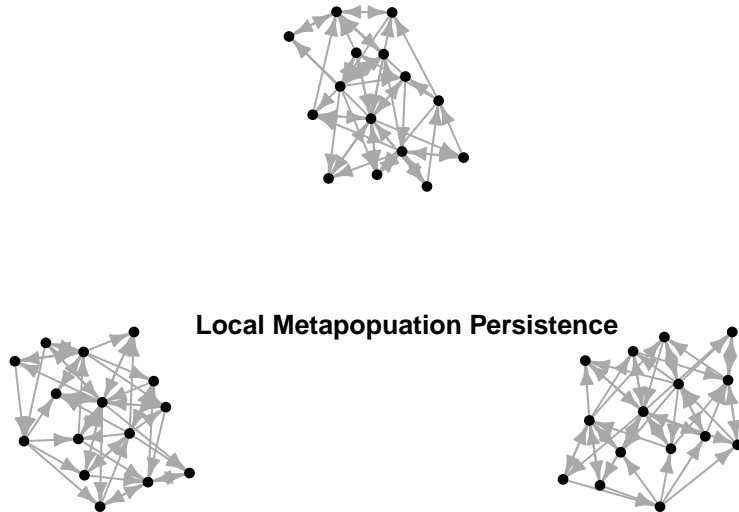
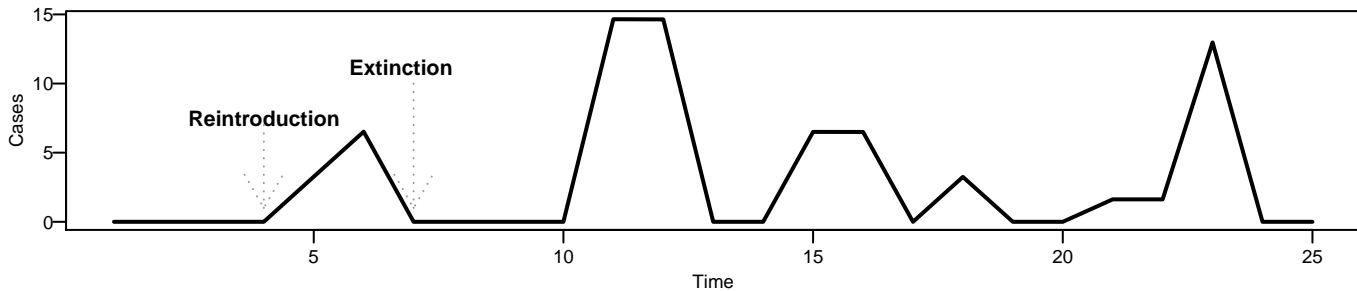
382

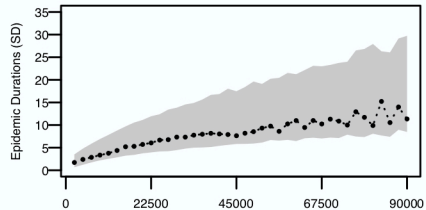
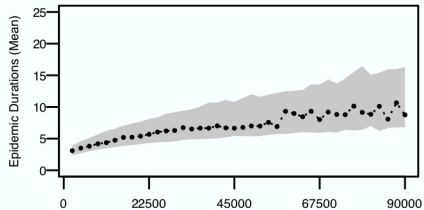
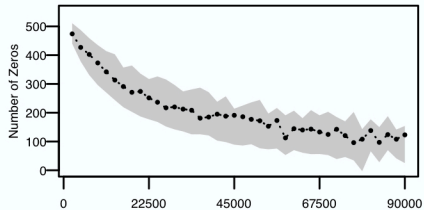
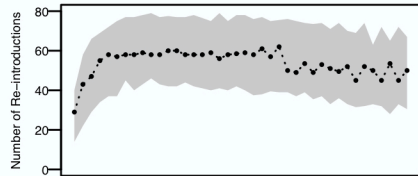
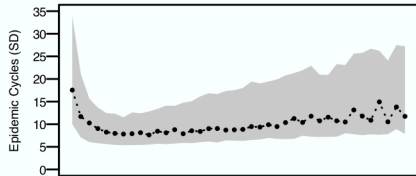
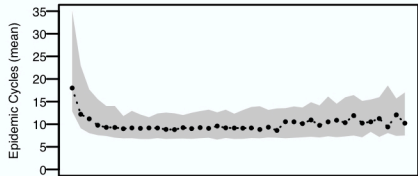
383 **Figure 3: Pre-vaccination regional dynamics of measles, inferred from the Absence-Presence-**
384 **Absence model in a competing-risks framework. a) The crude global distribution of risk of**
385 **reintroduction of infection due to *spatially predictable* (i.e. core-satellite plus LMP) *versus***
386 **unidentifiable random seeding. b) Spatial hotspot analysis using LISA (local indicators of spatial**
387 **association)^{21,23} revealing the *relative* importance of unidentifiable erratic spread in peripheral**
388 **areas. Filled red squares represent regions where the unidentifiable seeding is significantly**
389 **important (at a nominal two-sided 5%-level) *relative* to the average for E&W; filled grey squares**
390 **represent regions where gravity-driven patterns are significantly stronger. Geographical**
391 **locations: Norwich (NOR), London (LON), Manchester (MAN), Liverpool (LIV), Swansea**
392 **(SWA), Cardiff (CAR), Plymouth (PLY) and Truro (TRU). c) Relative importance of core cities.**
393 **The most influential city, which has the largest proportion of reintroductions (indicated by**
394 **bubble size) among all reintroductions in a recipient community due to hierarchical gravity**
395 **coupling, is shown. An “other” city/town (a black dot) represents a place other than the**
396 **considered core cities. d) The distribution of distance of spread from the most influential (non-**
397 **core) cities (black dots) in Figure 4c. The median distance of spread is 10.3 km with 95% C.I.**
398 **[2.0, 72.5].**
399

400

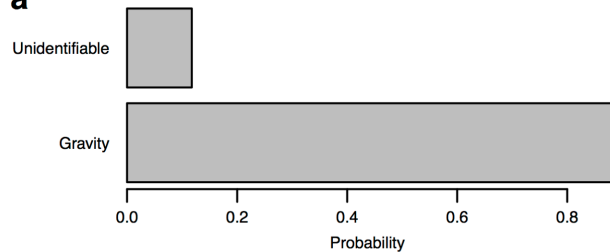
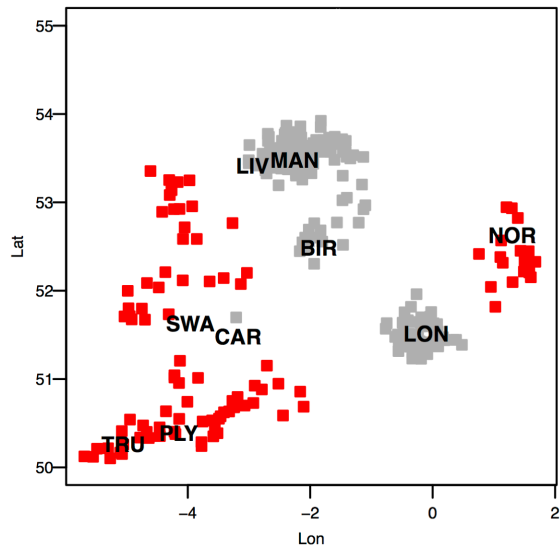
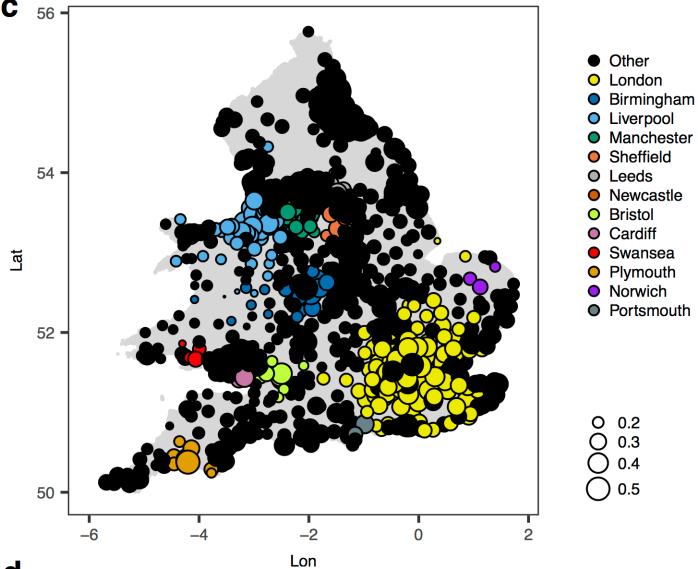
401 **Figure 4: Impact of vaccination on spatial spread of measles a) Location-wise risk distribution**
402 **for small places over the course of vaccine introduction and measles control in 5-year windows.**
403 **Size of a bubble indicates proportion of reintroductions due to the most impactful source of**
404 **infection (Gravity or Unidentifiable Seeding). Unidentifiable seeding became more widespread**
405 **(i.e. more black dots) and more prominent (i.e. larger sizes) with increasing vaccination cover. b)**
406 **Crude global risk distribution among unidentifiable *versus* gravity-driven seedings. The red line**
407 **represents average vaccination coverage. (c) Although we find high local and regional**
408 **synchrony⁴, as calculated by a nonparametric spatial correlation function²⁴, of epidemics in the**
409 **pre-vaccination era, asynchrony dominates during peak vaccination coverage as our model fails**
410 **to identify the majority of importations.**
411

412

a**b****c**



Average Population Level

a**b****c****d**